

Self-Adaptive Transfer Learning for Multicenter Glaucoma Classification in Fundus Retina Images

Yiming Bao, Jun Wang, Tong Li, Linyan Wang, Jianwei Xu, Juan Ye and Dahong Qian, *Senior Member, IEEE*

arXiv:2105.03068v1 [eess.IV] 7 May 2021

Abstract—The early diagnosis and screening of glaucoma are important for patients to receive treatment in time and maintain eyesight. Nowadays, deep learning (DL) based models have been successfully used for computer-aided diagnosis (CAD) of glaucoma from retina fundus images. However, a DL model pre-trained using a dataset from one hospital center may have poor performance on a dataset from another new hospital center and therefore its applications in the real scene are limited. In this paper, we propose a self-adaptive transfer learning (SATL) strategy to fill the domain gap between multicenter datasets. Specifically, the encoder of a DL model that is pre-trained on the source domain is used to initialize the encoder of a reconstruction model. Then, the reconstruction model is trained using only unlabeled image data from the target domain, which makes the encoder in the model adapt itself to extract useful high-level features both for target domain images encoding and glaucoma classification, simultaneously. Experimental results demonstrate that the proposed SATL strategy is effective in the domain adaptation task between a private and two public glaucoma diagnosis datasets, i.e. pri-RFG, REFUGE, and LAG. Moreover, the proposed strategy is completely independent of the source domain data, which meets the real scene application and the privacy protection policy.

Index Terms—Glaucoma Diagnosis, Transfer Learning, Multicenter Domain Adaptation

I. INTRODUCTION

GLAUCOMA is one of the most primary leading causes of blindness [1]. The loss of sight due to glaucoma is irreversible while some other eye diseases such as myopia

This work was supported in part by Department of Science and Technology of Zhejiang Province - Key Research and Development Program under Grant 2017C03029 and the Biomedical Engineering Interdisciplinary Research Fund of Shanghai Jiao Tong University under Grant YG2020YQ17.

Y. Bao and J. Wang are contributed equally in this work as co-first authors. J. Ye and D. Qian are contributed equally in this work as co-corresponding authors.

Y. Bao, J. Wang, Tong Li, Jianwei Xu and D. Qian are with the School of Biomedical Engineering, Shanghai Jiao Tong University, Shanghai, China (e-mail: yiming.bao@sjtu.edu.cn; wjcy19870122@163.com; tong.li@sjtu.edu.cn; jianwei.xu@sjtu.edu.cn; dahong.qian@sjtu.edu.cn)

J. Ye and Linyan Wang is with the Department of Ophthalmology, the Second Affiliated Hospital of Zhejiang University, College of Medicine, Hangzhou 310009, China (e-mail: yejuan@zju.edu.cn; wan-glinyan@zju.edu.cn)

and presbyopia are not. Thus, early diagnosis of glaucoma for effective treatment and vision conservation matters a lot for patients.

However, the symptoms of glaucoma in the early stage are difficult to perceive. One of the standard methods widely used by eye specialists nowadays is the optic nerve head (ONH) assessment [1] in fundus retina images. Whereas, mastering the tricks of performing ONH assessment remains challenging. It is time-consuming for one clinician to accumulate enough experience for screening and diagnosis. Therefore, some automatically calculated parameters were presented and popularized as quantitative clinical measurements, such as cup to disc ratio (CRD) which means the ratio of vertical cup diameter to vertical disc diameter in the fundus retina image. Generally, a larger CRD represents a higher possibility of glaucoma and vice versa. In recent years, some segmentation algorithms were proposed to extract the cup and the disc region from the fundus retina image, followed by the calculation of CRD and diagnosis of glaucoma. However, manually labeling the mask of the cup or disc region is labor-consuming, which makes image-level category labels necessary and reasonable for automatically screening glaucoma.

In the past several years, Deep Learning (DL) based methods have received unprecedented attention and achieved state-of-the-art performance in many fields, including medical image analysis [2]. Glaucoma can be screened from fundus retina images by DL models which are well trained on sufficient data and precise image-level labels [3]. However, DL models trained on one single site cannot be directly generalized and applied to other sites. In the real scene, the dataset in hands for testing the pre-trained model usually comes from a brand-new hospital. The distributions of training and testing data are partially different so the pre-trained model may fail to fulfill the required task.

Generally, the distribution of a medical image dataset relies on many factors, such as the specification of instruments and scanners, external environment during imaging and internal parameters for reconstruction, or other scanning protocols. The discrepancy between images from different sites can be reflected in many image statistical traits, such as color style, contrast, resolution, and so on.

Commonly, the difference between datasets can be seen as a domain gap. To be specific, the joint distributions of data

and labels are different between the source and the target domain, i.e., $P(x^s, y^s) \neq P(x^t, y^t)$. This is mainly because the margin distributions are different, i.e., $P(x^s) \neq P(x^t)$ while the conditional distributions, i.e., $P(y^s|x^s)$ and $P(y^t|x^t)$ are similar. Many methods have been proposed to solve this problem. Fine tuning [4] is most widely used in real practical applications. However, fine-tuning cannot fill up all domain gaps. Sometimes, the dataset from a new target domain is completely unlabeled so that fine-tuning is unable to apply.

Another way to solve the domain gap problem is called transfer adaptation learning (TAL) [5], [6], which is a combination of transfer learning (TL) and domain adaptation (DA). Recently, TAL is becoming increasingly popular in the medical imaging community. It can be categorized into three classes as follows:

(1) Instance Re-weighting Adaptation Learning (IRAL) [7]–[9]. Methods in this area assign weights to the source domain instances based on their similarity to the target domain instances. Via re-sampling or importance weighting, the performance of the trained source classifier in the target domain can be enhanced. However, the estimation of the assigned weights is under a prior-decided parametric distribution assumption [5], which may differ from the true parametric distribution.

(2) Feature Adaptation Learning (FAL) [10]–[19]. For adapting datasets from multiple domains, methods in this category are widely proposed to find a feature representation space where the projected features from target and source domain follow similar distributions. In the past few years, the most famous FAL methods are GAN-based domain adaptation models. However, Several drawbacks restrict the development of GAN models in medical image analysis. First, finding a general feature space for most domains remains challenging. Second, training a GAN-based domain adaptation model needs both source and target domain data, which is more and more impractical in the real scene due to the privacy protection policy for medical data.

(3) Self-Supervised Transfer Learning (SSTL) [20]–[32]. Algorithms in this category focus on training a supervised classifier on the source domain and then transfer its knowledge to the target domain via self-supervised learning. For example, Cheng *et al* [21] proposed a multimodal manifold-regularized transfer learning method for Alzheimer’s disease(AD) and mild cognitive impairment (MCI) using data from different domains. Cheplygina *et al* [22] investigated a Gaussian texture features-based classification model of chronic obstructive pulmonary disease(COPD) in a multicenter dataset with scans from three different centers, four different scanners, with heterogeneous subject distribution. These methods integrate the data information from different domains by extracting some manually designed features from images, which is short of generalization ability and not suitable for unseen domains.

To solve the above-mentioned challenges in solving the domain gap problem, a novel multi-stage framework is proposed in this paper for domain adaptation of glaucoma classification. Specifically, we train a convolutional neural network in the source domain with sufficient labeled data for glaucoma classification. Then, the feature extraction part of the trained model is shared as the encoder of a reconstruction network. The

reconstruction model is trained using only unlabeled data in the target domain to adapt itself. Finally, the adapted encoder of this reconstruction model is utilized in the target domain and generates weak labels. We call the proposed framework *self-adaptive transfer learning* (SATL). It is supposed that the self-adapted model will have both the feature learning ability for glaucoma classification and the distribution fitting ability of the target domain for domain adaptation. The contributions of this paper can be concluded as follows:

(1) To the best of our knowledge, our work is the first to investigate the study of transfer adaptation learning for the classification of glaucoma with multicenter fundus retina images.

(2) Our method trains a classification model in the source domain and then transfers this model to the target domain without using any data in the source domain. A self-adaptive reconstruction model is trained only using unlabeled images in the target domain, which guarantees the security and privacy of different datasets. Our strategy can make sure the datasets from multiple hospitals fully independent so it has great potential for real scene applications.

(3) Experimental results shows that our method can preserve most of the classification ability of the off-shelf model from one hospital to another and meanwhile furthermore improve its performance. Even totally independent from source domain data, it outperforms other domain adaptation method such as CycleGAN, which heavily relies on source domain data in the training stage.

II. METHOD

In this section, we describe our proposed strategy for solving the problem of domain adaptation in multicenter glaucoma classification based on fundus retina images, which we refer to as (Self-Adaptive Transfer Learning) (SATL). First, we state the problem of domain adaptation. Then, the main framework of our method is introduced, with new designed convolutional neural network and loss functions.

A. Problem Statement

In general, the domain adaptation techniques are mostly used for lifting the generalization ability of the source model and performing pseudo label in unseen domains. We can define a domain as a joint probability distribution $\mathcal{P}_{\mathcal{X}, \mathcal{Y}}$ on \mathcal{X} and \mathcal{Y} where \mathcal{X} is the input space and \mathcal{Y} is the output space. Denote the source domain by \mathcal{M} and the target domain by \mathcal{N} , where $\mathcal{M} \neq \mathcal{N}$. The main destination of domain adaptation in this paper can be described as follows: given labeled samples from a source domain and unlabeled samples from a target domain:

$$S^s = (x_i^s, y_i^s)_{i=1}^{n_s} \sim \mathcal{M}, S_u^t = (x_i^t)_{i=1}^{n_t} \sim \mathcal{N} \quad (1)$$

, find a good labeling function $f: \mathcal{X} \rightarrow \mathcal{Y}$ on S_u^t . Directly forming this labeling function is challenging due to the high dimension of input space. Thus, a feature learning approach is used in this paper by designing a convolutional neural network. The labeling function can be denoted as: $f: \mathcal{X} \rightarrow \mathcal{F} \rightarrow \mathcal{Y}$, where \mathcal{F} represents the feature space.

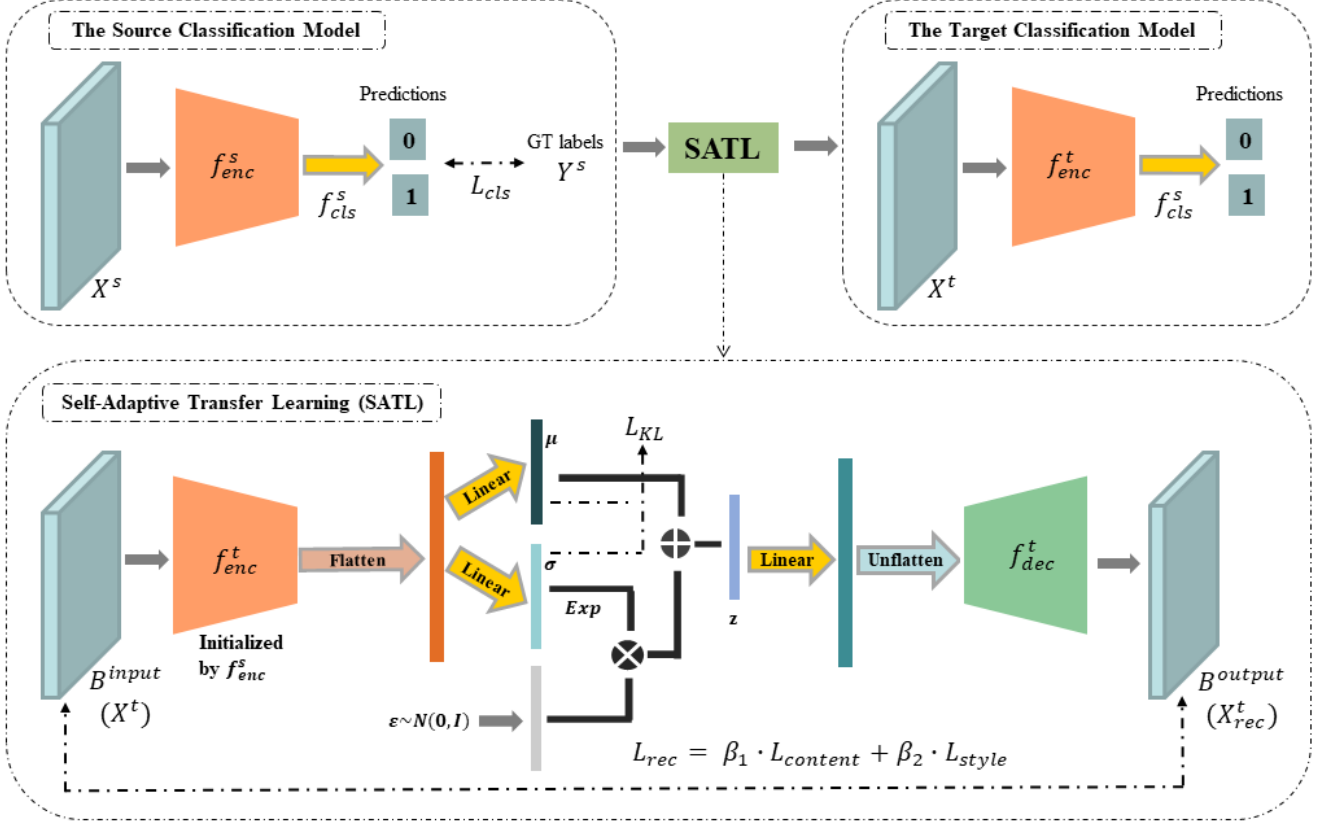


Fig. 1. Illustration of the proposed self-adaptive transfer learning (SATL) strategy. As shown at the top left of the image, a classification model for glaucoma screening is pre-trained using labeled data from the source domain via a fully supervised way. Through the SATL framework, a new classification model turns out to perform well in the target domain. As shown at the below of the image, in the SATL framework, f_{enc}^s of the source classification model is used to initialize f_{enc}^t of a reconstruction model which is implemented as a variational auto-encoder (VAE). The VAE is trained using only unlabeled images from the target domain to self-adapt f_{enc}^t , which is then used to build the target classification model with the pre-trained lightweight classifier f_{cls}^s . The proposed framework is independent of the source domain data, which is more suitable for the real scene applications.

In practice, the feature representation function, $f_{enc} : \mathcal{X} \rightarrow \mathcal{F}$, which is well-trained on a source domain, can model the data information in latent space. Simultaneously, the classification function $f_{cls} : \mathcal{F} \rightarrow \mathcal{Y}$ can model the label information.

However, when transferred to a target domain, f_{enc} is unable to model the information of unseen images, which is the main challenge in the transfer learning field. Therefore, the features \mathcal{F} fed into f_{cls} is not suitable and feasible for classification. To adapt f_{enc} to make it able to encode the information of images from a target domain, a new reconstruction model with novel loss functions is proposed in this paper, which uses only unlabeled image data in the target domain. The reconstruction model is implemented as a variational auto-encoder (VAE) [33]. The above-mentioned framework is referred to as self-adaptive transfer learning (SATL) and the detail of it will be introduced in the next subsection.

B. Self-Adaptive Transfer Learning (SATL)

The framework of the proposed method is illustrated in Fig. 1. The proposed SATL framework can transfer a pre-trained source classification model to a target domain without using neither source images nor labels.

Let $f^s : \mathcal{X}^s \rightarrow \mathcal{Y}^s$ be the source pre-trained classification model and $f^t : \mathcal{X}^t \rightarrow \mathcal{X}_{rec}^t$ be the target reconstruction model. The feature encoder is denoted as $f_{enc} : \mathcal{X} \rightarrow \mathcal{F}$ and the lightweight classification function $f_{cls} : \mathcal{F} \rightarrow \mathcal{Y}$. We denote one more function: an decoder $f_{dec} : \mathcal{F} \rightarrow \mathcal{X}$ in f^t . Then, given an input sample x , f^s and f^t can be formulated as :

$$f^s(x) = f_{cls}^s(f_{enc}^s(x)), \quad (2)$$

$$f^t(x) = f_{dec}^t(f_{enc}^t(x)) \quad (3)$$

Once $f^t(x)$ is trained, we can build the self-adapted classification model $f_{SA}^t(x)$ for target domain image classification, which can encode the information of images from the target domain.

$$f_{SA}^t(x) = f_{cls}^s(f_{enc}^t(x)) \quad (4)$$

Let $\Theta^s = \{\Theta_{enc}^s; \Theta_{cls}^s\}$ and $\Theta^t = \{\Theta_{enc}^t; \Theta_{dec}^t\}$ denote the parameters of f^s and f^t , respectively. A variational auto-encoder (VAE), which can compress the image information and sample a latent vector z , is implemented and trained using only unlabeled images in the target domain. As shown in Fig. 1, the encoder of this reconstruction model f_{enc}^t is

TABLE I
THE STATISTICAL DIFFERENCE BETWEEN THREE DATASETS

Dataset	Domain	Number of samples	Positive vs. Negative	Average of image size	Release year
LAG (public)	Source / Target	4854	3143:1689	300 × 300	2019
pri-RFG (private)	Source / Target	1881	1013 : 868	989 × 989	-
REFUGE (public)	Target only	400	40 : 360	1062 × 1062	2020

initialized by the pre-trained source encoder f_{enc}^s . Then, the output feature map of f_{enc}^t is flattened. Two linear layers are followed to get vectors μ_n and σ_n , which are utilized to re-sample a latent vector z_n , where n is the input batch size, μ_n is the mean of z_n and σ is the variation of the noise in z_n . Moreover, another n -dimension vector $\varepsilon \sim N(0, 1)$ is sampled as a noise. Finally, the latent vector z_n can be re-sampled as:

$$z_n = \mu_n + \varepsilon_n \times \exp(\sigma_n) \quad (5)$$

The latent vector is then unflattened and decoded into a batch of output images that have the same image size and channels with the batch of input images. The loss function used to optimize the proposed self-adaptive model can be represented as:

$$L(\Theta_{enc}^t, \Theta_{dec}^t, x^t) = \alpha \cdot L_{KL} + \beta \cdot L_{rec}, \quad (6)$$

$$L_{KL} = -\alpha \cdot KL(f_{enc}^t(z|x^t) | f_{dec}^t(z|x^t)), \quad (7)$$

where the first term in the loss function is the KL divergency of the latent vector distribution and the true data distribution, which is simplified as L_{KL} . The second term L_{rec} is the reconstruction loss between the output image and the input image. Instead using a single MSE loss, we perform a new designed combination of two loss functions [34]. We argue that the self-adaptive reconstruction model should be guided to reconstruct high-level style information in the target domain images rather than just the pixel-wise texture. Thus, the reconstruction loss function designed in this paper is as follows:

$$\begin{aligned} L_{rec} &= \beta_1 \cdot L_{content} + \beta_2 \cdot L_{style} \\ &= \beta_1 \cdot \sum_{i,j,k} (B_{ijk}^{output} - B_{ijk}^{input})^2 \\ &\quad + \beta_2 \cdot \sum_{m,n} (G_{mn}^{output} - G_{mn}^{input})^2, \end{aligned} \quad (8)$$

where B^{output} and B^{input} denote the output and input image of the reconstruction model, respectively. i, j, k represent the position index of images. G^{output} and G^{input} are the Gram matrixes of B^{output} and B^{input} . m, n represents the index of matrixes. The gram matrix can be calculated by

$$G = \frac{1}{n_c \times n_h \times n_w} \mathbf{v} \mathbf{v}^T, \quad (9)$$

where \mathbf{v} is the flattened column vector of B^{output} or B^{input} and n_c represents the image channels n_h, n_w represent the image size.

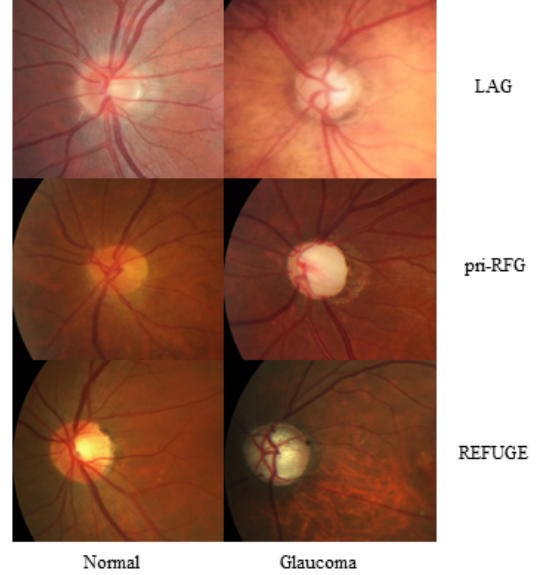


Fig. 2. Normal and glaucoma examples from different datasets. Image statistical traits such as color style, contrast, resolution are quite different between retina fundus images in three used datasets.

III. EXPERIMENTS AND RESULTS

A. Datasets

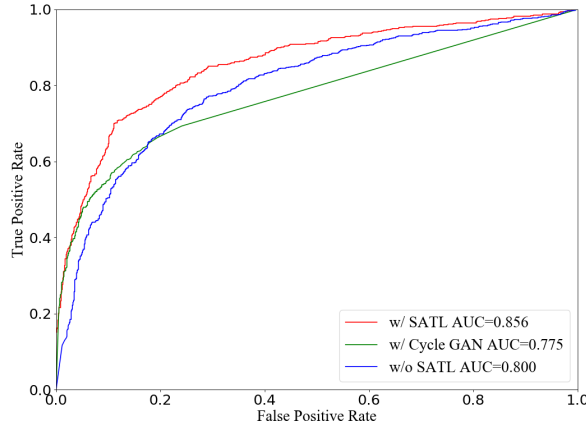
We used two public datasets and one private dataset to validate the method proposed in this paper. The first public dataset is large-scale attention-based glaucoma(LAG) dataset [35] established by Li *et al.* The second public dataset is from the REFUGE challenge [36]. Moreover, we also collected 1881 retina fundus images from The Second Affiliated Hospital of Zhejiang University and built a private dataset (pri-RFG) via labeling all the images with and without glaucoma by experienced ophthalmologists.

The details of the above-mentioned three datasets (LAG, REFUGE, pri-RFG) are summarized and tabulated in Table I. By observing the dataset statistics, we can find the scales and the average size of images in the three used datasets are quite various. Also, they all have different levels of imbalance of glaucoma and normal samples. These distinctions make transfer learning between them challenging.

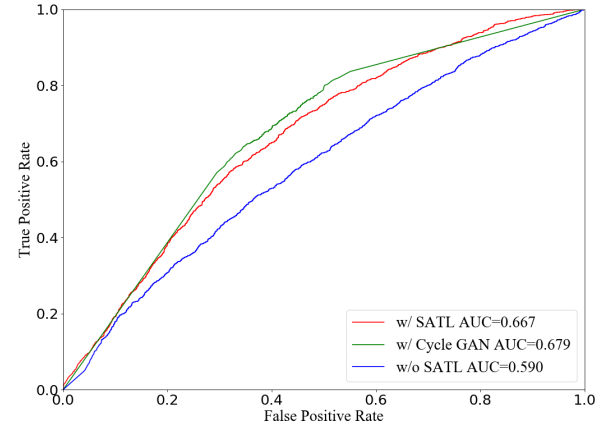
In Fig. 2, we illustrate some normal and glaucoma examples in three used datasets. The image style and other image attributes between them are visibly distinguished. Due to the image distinctions between datasets in several aspects, a glaucoma classification model trained on one dataset may

TABLE II
THE CLASSIFICATION PERFORMANCE OF FOUR GROUPS OF EXPERIMENTS

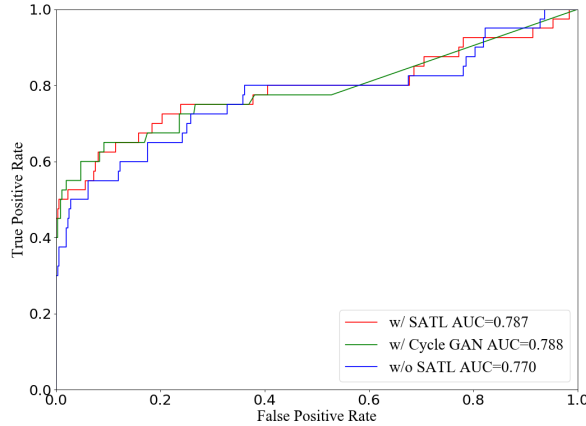
LAG → pri-RFG			pri-RFG → LAG			LAG → REFUGE			pri-RFG → REFUGE			
w/o SATL	w/ CycleGAN	w/ SATL	w/o SATL	w/ CycleGAN	w/ SATL	w/o SATL	w/ CycleGAN	w/ SATL	w/o SATL	w/ CycleGAN	w/ SATL	
Accuracy	0.799	0.672	0.856	0.352	0.628	0.579	0.933	0.913	0.945	0.240	0.540	0.580
Recall	0.659	0.422	0.726	1.000	0.707	0.779	0.425	0.600	0.500	0.975	0.825	0.850
Precision	0.807	0.923	0.855	0.352	0.481	0.445	0.810	0.558	0.909	0.114	0.157	0.173
F1 Score	0.726	0.580	0.785	0.521	0.573	0.566	0.557	0.579	0.645	0.204	0.264	0.288



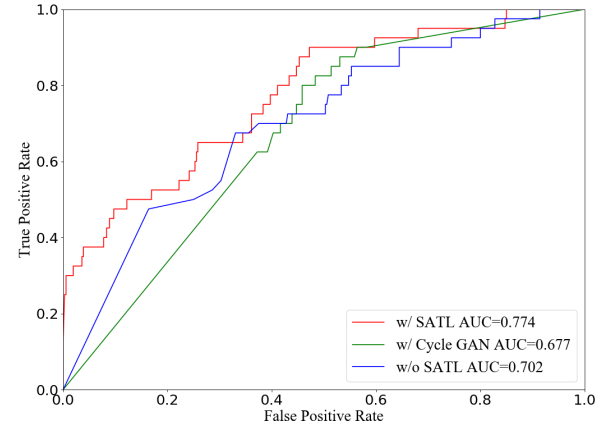
(a) LAG → pri-RFG



(b) pri-RFG → LAG



(c) LAG → REFUGE



(d) pri-RFG → REFUGE

Fig. 3. ROC curves of the models evaluated in all four domain adaptation directions.

achieve unsatisfied performance on another dataset, even if we normalize the images with technique such as intensity histogram match between feeding them into pre-trained model. Therefore, the value of the pre-trained model decreases. The applications of deep learning models in computer-aided diagnosis are also limited.

Due to the limitation of sample number in dataset REFUGE, we just used it as target domain to evaluate the SATL strategy, while another public dataset LAG and the private dataset pri-RFG are used for cross-domain evaluation. In other words, we implemented a total of four groups of experiments. Based on the direction from source domain to target domain, the four

domain adaptation experimental groups can be represented as LAG → pri-RFG, pri-RFG → LAG, LAG → REFUGE and pri-RFG → REFUGE.

B. Implement Details and Evaluation Metrics

Both the source classification model and the target reconstruction model were implemented using Pytorch (version 1.3.0) and trained on an NVIDIA RTX 2080Ti GPU. We implemented the source classification model as a VGG [37] and optimized it with cross entropy (CE) loss [38]. During the training stage of the source classification model, we set

the learning rate as 10^{-6} , weight decay as 5×10^{-4} . All the samples in the source domain were split into training set and validation set using a ratio of 7 : 3, following stratified sampling method to ensure that the pos vs. neg ratios in each set are similar. At each iteration, a mini-batch of 16 samples were fed into the model. The number of training epochs was set as 50. To avoid the over-fitting issue, the model which achieved the maximum accuracy in the validation set was saved.

During the training stage of the target self-adaptive reconstruction model, the encoder of the model was initialized as the encoder of the source classification model. The learning rate of the encoder in the reconstruction model was set as 10^{-7} and that of the rest part was set as 10^{-3} . To make the reconstruction model better see the whole statistical traits of the target domain images and self-adapt its encoder, we used all the image samples in the target domain for training. To avoid over-fitting the reconstruction task and losing the ability to extract features that are useful for classification task, the target reconstruction model was trained only 20 epochs. We empirically set the weights α , β_1 and β_2 in the reconstruction loss function as 0.3, 0.2, 0.5. The channel number of the latent vector in the reconstruction VAE model was set as 32. Both the channel number of the latent vector and the loss function weights will be evaluated and discussed in section IV.

Once the target reconstruction model was trained, the self-adapted encoder of it was used as the feature extractor of a target classification model. The last FC layer of the source classification model played a role as the feature classifier. This new combined target classification model was evaluated by metrics in terms of accuracy, recall, precision, f1 score and area under the ROC curve (AUC).

C. Results

As described in Section III-B, based on the three available datasets, there are four executable domain adaptation directions. They are denoted as LAG \rightarrow pri-RFG, pri-RFG \rightarrow LAG, LAG \rightarrow REFUGE, and pri-RFG \rightarrow REFUGE. For evaluating the proposed SATL strategy, we conducted experiments in each direction and compared its performance to that of the source classification model and a state-of-the-art CycleGAN-based domain adaptation method [39]. The CycleGAN-based method trains a generator to transfer the target images to the source domain by adversarial learning. The most noteworthy difference between CycleGAN and the proposed SATL strategy is that: our method is completely independent of the source domain data while CycleGAN is not. More specifically, training CycleGAN to perform domain adaptation needs both source and target domain images. On the contrary, the proposed SATL strategy relies on only the target domain unlabeled images.

The experimental results of the classification model without SATL, with SATL and with CycleGAN are tabulated in Table II. Moreover, the ROC curves are also plotted and illustrated in Fig. 3.

By observing the demonstrated results in Table II and Fig. 3, two main conclusions can be drawn:

(1) Compared to the source model without SATL, which can be seen as a baseline, the model with SATL outperforms in all four domain adaptation directions. Despite there exist a mass of differences between three used datasets, SATL shows to be effective for self-supervised domain adaptation regardless of the source and target domain data distribution. This phenomenon shows that the proposed SATL is valuable and reliable for the production of pseudo labels in an unseen domain.

(2) When testing the source model in the target domain images transferred by CycleGAN, the performance is comparable with the proposed SATL strategy in domain adaptation directions of pri-RFG \rightarrow LAG and LAG \rightarrow REFUGE. While in directions of LAG \rightarrow pri-RFG and pri-RFG \rightarrow REFUGE, the proposed SATL strategy surpasses the CycleGAN by a large margin. This phenomenon demonstrates that SATL is more robust and have more stable generalization ability in different domain adaptation scene. Note that CycleGAN even uses the source domain images to help the training process. Thus, our method which is completely independent of the source domain is more feasible in real scene applications. It can ensure the isolation of multi-center datasets and meet the privacy protection policy.

IV. DISCUSSION

The early diagnosis of glaucoma is important for clinical treatment, so a high-accuracy automatic classification method is highly demanded in real scene screening. Although many methods based on deep learning were developed for this problem, there still exists a gap between well-trained deep learning models and clinical practice due to the domain shift and the lack of annotations in a new domain. In this paper, we proposed a new self-supervised domain adaptation method called self-adaptive transfer learning (SATL) to solve this problem without using any source domain images. The main inspiration of our method is to make the encoder of the classification model adapt itself to the target domain. A reconstruction model, which is implemented as a VAE, was trained using only target domain unlabeled images.

Experimental results show that the proposed SATL strategy outperforms both the baseline and other state-of-the-art domain adaptation method CyclyGAN which even uses the source domain images. Based on three available datasets, four domain adaptation directions are explored and evaluated. The proposed SATL proved to be effective and robust in all directions, which demonstrated it has stable generalization ability between domains.

Two key factors need to be decided in the proposed SATL strategy. One of them is the channel number z of the latent vector in the reconstruction VAE model. We choose the domain adaptation between two public datasets LAG and REFUGE to conduct and evaluate the ablation study of z . Fig. 4 shows the use of $z=32$ achieves the highest classification performance compared to other numbers. When the number of z was >32 , the AUC decrease. While a larger number of z may bolster the ability of VAE to store information of images, the model may under-fit the reconstruction task thus fail to extract

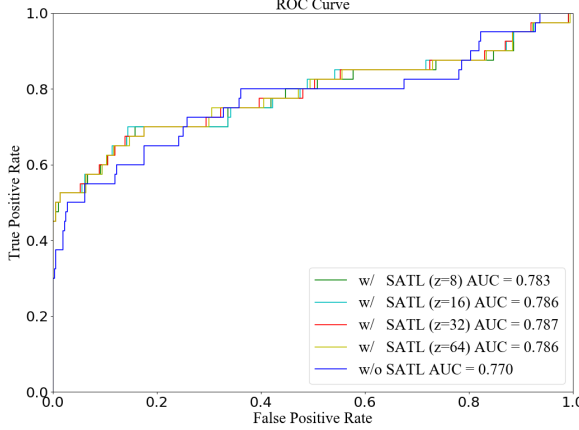


Fig. 4. ROC curves of choosing the channel number z of the latent vector.

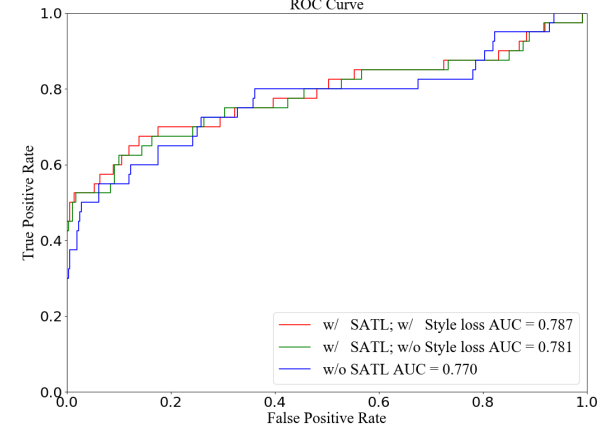


Fig. 5. ROC curves of ablation study on designed style loss.

image features in the target domain. Another factor worth analyzing is the combined loss functions in the reconstruction VAE. Fig. 5 shows the ablation study of the designed style loss. When performing domain adaptation without style loss, the AUC score decreases. It is mainly because when the reconstruction VAE is optimized using only content loss, it may primarily concentrate on the pixel-level features while ignoring the image texture features or the style of target domain images. In this paper, we integrated content loss with style loss using fixed weights. However, the weights can be furthermore analyzed and discussed in future work. Moreover, other kinds of losses can be researched and carefully designed for the self-supervised domain adaptation task.

Despite the proposed method improves the performance of the classification model in the target domain via self-supervised training, there still remains some research worth exploring for enhancing the performance. For example, in this paper, we directly trained and validated the source classification model on the source domain. However, it may be a better option to initialize the source classification model by a model pre-trained on large scale nature image datasets such as ImageNet. Besides, the backbone used in this paper is VGG for the convenience of building the reconstruction VAE model. In the future, it can also be replaced by other state-of-the-art backbone such as Inception [40] or SENet [41]. However, how to implement the decoder and ensure the symmetry of VAE when utilizing other backbones needs to explore, too.

V. CONCLUSION

In this paper, we present a self-adaptive transfer learning (SATL) strategy to fill the domain gap between multicenter datasets and perform the evaluation in glaucoma classification based on three fundus retina image datasets. Specifically, a reconstruction model is trained using only target domain unlabeled images. The encoder of this reconstruction model is initialized from a pre-trained source classification model and self-adapted in the target domain. Experimental results demonstrate that the proposed SATL strategy enhances the classi-

fication performance in the target domain and outperforms another state-of-the-art domain adaptation method which even utilizes source domain images for training, as well. In the near future, more efforts will be devoted to exploring how to furthermore lifting the performance of the self-supervised domain adaptation method via designing new reconstruction losses. Moreover, we will extend this strategy to other medical image analysis problems.

REFERENCES

- [1] M. C. V. S. Mary, E. B. Rajsingh, and G. R. Naik, "Retinal fundus image analysis for diagnosis of glaucoma: A comprehensive survey," *IEEE Access*, vol. 4, pp. 4327–4354, 2016.
- [2] D. Ravi, C. Wong, F. Deligianni, M. Berthelot, J. Andreuperez, B. Lo, and G. Yang, "Deep learning for health informatics," vol. 21, no. 1, pp. 4–21, 2017.
- [3] H. Fu, J. Cheng, Y. Xu, C. Zhang, D. W. K. Wong, J. Liu, and X. Cao, "Disc-aware ensemble network for glaucoma screening from fundus image," *IEEE Transactions on Medical Imaging*, vol. 37, no. 11, pp. 2493–2501, 2018.
- [4] N. Tajbakhsh, J. Y. Shin, S. R. Gurudu, R. T. Hurst, C. B. Kendall, M. B. Gotway, and J. Liang, "Convolutional neural networks for medical image analysis: Full training or fine tuning?," *IEEE Transactions on Medical Imaging*, vol. 35, no. 5, pp. 1299–1312, 2016.
- [5] L. Zhang, "Transfer adaptation learning: A decade survey.," *arXiv: Computer Vision and Pattern Recognition*, 2019.
- [6] M. Wang and W. Deng, "Deep visual domain adaptation: A survey," *Neurocomputing*, vol. 312, pp. 135–153, 2018.
- [7] G. Quellec, G. Cazuguel, B. Cochener, and M. Lamard, "Multiple-instance learning for medical image and video analysis," *IEEE Reviews in Biomedical Engineering*, vol. 10, pp. 213–234, 2017.
- [8] Q. Zhu, B. Du, and P. Yan, "Boundary-weighted domain adaptive neural network for prostate mr image segmentation," *IEEE Transactions on Medical Imaging*, vol. 39, no. 3, pp. 753–763, 2020.
- [9] Q. Qi, Y. Li, J. Wang, H. Zheng, Y. Huang, X. Ding, and G. K. Rohde, "Label-efficient breast cancer histopathological image classification," *IEEE Journal of Biomedical and Health Informatics*, vol. 23, no. 5, pp. 2108–2116, 2019.
- [10] E. Ahn, A. Kumar, M. J. Fulham, D. Feng, and J. Kim, "Convolutional sparse kernel network for unsupervised medical image analysis," *Medical Image Analysis*, vol. 56, pp. 140–151, 2019.
- [11] T. Zhang, J. Cheng, H. Fu, Z. Gu, Y. Xiao, K. Zhou, S. Gao, R. Zheng, and J. Liu, "Noise adaptation generative adversarial network for medical image analysis," *IEEE Transactions on Medical Imaging*, no. 99, pp. 1–1, 2019.

[12] F. Mahmood, R. J. Chen, and N. J. Durr, "Unsupervised reverse domain adaptation for synthetic medical images via adversarial training," *IEEE Transactions on Medical Imaging*, vol. 37, no. 12, pp. 2572–2581, 2018.

[13] R. Bermudezchacon, O. Altingovde, C. Becker, M. Salzmann, and P. Fua, "Visual correspondences for unsupervised domain adaptation on electron microscopy images," *IEEE Transactions on Medical Imaging*, pp. 1–1, 2019.

[14] D. P. Kingma, S. Mohamed, D. J. Rezende, and M. Welling, "Semi-supervised learning with deep generative models," vol. 27, pp. 3581–3589, 2014.

[15] S. Wang, L. Yu, X. Yang, C. Fu, and P. Heng, "Patch-based output space adversarial learning for joint optic disc and cup segmentation," *IEEE Transactions on Medical Imaging*, vol. 38, no. 11, pp. 2485–2495, 2019.

[16] P. Costa, A. Galdran, M. I. Meyer, M. Niemeijer, M. D. Abramoff, A. M. Mendonca, and A. Campilho, "End-to-end adversarial retinal image synthesis," *IEEE Transactions on Medical Imaging*, vol. 37, no. 3, pp. 781–791, 2018.

[17] M. W. Lafarge, J. P. W. Pluim, K. A. J. Eppenhof, and M. Veta, "Learning domain-invariant representations of histological images," *Frontiers in Medicine*, vol. 6, p. 162, 2019.

[18] Q. Dou, D. C. Castro, K. Kamnitsas, and B. Glocker, "Domain generalization via model-agnostic learning of semantic features," pp. 6450–6461, 2019.

[19] Y. Shen, B. Sheng, R. Fang, H. Li, L. Dai, S. Stolte, J. Qin, W. Jia, and D. Shen, "Domain-invariant interpretable fundus image quality assessment," *Medical Image Analysis*, vol. 61, p. 101654, 2020.

[20] M. Ghifary, W. B. Kleijn, M. Zhang, D. Balduzzi, and W. Li, "Deep reconstruction-classification networks for unsupervised domain adaptation," pp. 597–613, 2016.

[21] B. Cheng, M. Liu, H. Suk, D. Shen, and D. Zhang, "Multimodal manifold-regularized transfer learning for mci conversion prediction," *Brain Imaging and Behavior*, vol. 9, no. 4, pp. 913–926, 2015.

[22] V. Cheplygina, I. P. Pena, J. H. Pedersen, D. A. Lynch, L. Sorensen, and M. De Bruijne, "Transfer learning for multicenter classification of chronic obstructive pulmonary disease," *IEEE Journal of Biomedical and Health Informatics*, vol. 22, no. 5, pp. 1486–1496, 2018.

[23] Y. Huang, H. Zheng, C. Liu, X. Ding, and G. K. Rohde, "Epithelium-stroma classification via convolutional neural networks and unsupervised domain adaptation in histopathological images," *IEEE Journal of Biomedical and Health Informatics*, vol. 21, no. 6, pp. 1625–1632, 2017.

[24] Y. Li, N. Wang, J. Shi, X. Hou, and J. Liu, "Adaptive batch normalization for practical domain adaptation," *Pattern Recognition*, vol. 80, pp. 109–117, 2018.

[25] W. Chang, T. You, S. Seo, S. Kwak, and B. Han, "Domain-specific batch normalization for unsupervised domain adaptation," pp. 7354–7362, 2019.

[26] C. Becker, C. M. Christoudias, and P. Fua, "Domain adaptation for microscopy imaging," *IEEE Transactions on Medical Imaging*, vol. 34, no. 5, pp. 1125–1139, 2015.

[27] S. Roy, A. Siarohin, E. Sangineto, S. R. Bulo, N. Sebe, and E. Ricci, "Unsupervised domain adaptation using feature-whitening and consensus loss," pp. 9471–9480, 2019.

[28] A. Noguchi and T. Harada, "Image generation from small datasets via batch statistics adaptation," *arXiv: Computer Vision and Pattern Recognition*, 2019.

[29] E. Ahn, A. Kumar, M. J. Fulham, D. Feng, and J. Kim, "Unsupervised domain adaptation to classify medical images using zero-bias convolutional auto-encoders and context-based feature augmentation," *IEEE Transactions on Medical Imaging*, pp. 1–1, 2020.

[30] A. Rozantsev, M. Salzmann, and P. Fua, "Beyond sharing weights for deep domain adaptation," *IEEE Transactions on Pattern Analysis and Machine Intelligence*, vol. 41, no. 4, pp. 801–814, 2019.

[31] N. Karani, K. Chaitanya, C. F. Baumgartner, and E. Konukoglu, "A lifelong learning approach to brain mr segmentation across scanners and protocols," pp. 476–484, 2018.

[32] S. Ioffe and C. Szegedy, "Batch normalization: Accelerating deep network training by reducing internal covariate shift," *arXiv: Learning*, 2015.

[33] D. P. Kingma and M. Welling, "Auto-encoding variational bayes," *arXiv: Machine Learning*, 2013.

[34] Y. Li, N. Wang, J. Liu, and X. Hou, "Demystifying neural style transfer," *arXiv: Computer Vision and Pattern Recognition*, 2017.

[35] L. Li, M. Xu, X. Wang, L. Jiang, and H. Liu, "Attention based glaucoma detection: A large-scale database and cnn model," *arXiv: Computer Vision and Pattern Recognition*, 2019.

[36] J. I. Orlando, H. Fu, J. B. Breda, K. Van Keer, D. R. Bathula, A. Diazpinto, R. Fang, P. Heng, J. Kim, J. Lee, *et al.*, "Refuge challenge: A unified framework for evaluating automated methods for glaucoma assessment from fundus photographs," *Medical Image Analysis*, vol. 59, p. 101570, 2020.

[37] K. Simonyan and A. Zisserman, "Very deep convolutional networks for large-scale image recognition," 2014.

[38] S. Ng and P. Perron, "Lag length selection and the construction of unit root tests with good size and power," *Econometrica*, vol. 69, no. 6, pp. 1519–1554, 2001.

[39] J. Zhu, T. Park, P. Isola, and A. A. Efros, "Unpaired image-to-image translation using cycle-consistent adversarial networks," pp. 2242–2251, 2017.

[40] C. Szegedy, S. Ioffe, V. Vanhoucke, and A. A. Alemi, "Inception-v4, inception-resnet and the impact of residual connections on learning," pp. 4278–4284, 2016.

[41] J. Hu, L. Shen, S. Albanie, G. Sun, and E. Wu, "Squeeze-and-excitation networks," *IEEE Transactions on Pattern Analysis and Machine Intelligence*, pp. 1–1, 2019.